Atmospheric Research xxx (2010) xxx–xxx

Contents lists available at ScienceDirect

Atmospheric Research

journal homepage: www.elsevier.com/locate/atmos

Raindrop size distributions of convective rain over equatorial Indonesia during the first CPEA campaign

Marzuki [a,d,*], Toshiaki Kozu [b], Toyoshi Shimomai [b], Hiroyuki Hashiguchi [c], Walter L. Randeu [a], Mutya Vonnisa [b]

[a] Institute of Broadband Communication, Graz University of Technology, Austria
[b] Interdisciplinary Faculty of Science and Engineering, Shimane University, Japan
[c] Research Institute for Sustainable Humanosphere (RISH), Kyoto University, Japan
[d] Department of Physics, Andalas University, Padang, Indonesia

ARTICLE INFO

Article history:
Received 4 August 2009
Received in revised form 18 February 2010
Accepted 1 March 2010
Available online xxxx

Keywords:
Raindrop size distribution
Instraseasonal variation
Kototabang

ABSTRACT

As part of the Coupling Processes in the Equatorial Atmosphere (CPEA) campaign, precipitation was observed at Kototabang (0.20°S, 100.32°E), Indonesia, by a 2D-Video Disdrometer (2DVD), a 1.3-GHz wind profiler, an Equatorial Atmosphere Radar (EAR) and a Mobile Automatic Weather Station (MAWS). The campaign period is from April 10 to May 9, 2004. This paper presents a comprehensive follow-up of the previous study on the intraseasonal variation (ISV) of raindrop size distribution (DSD) during this campaign. The data were partitioned into stratiform, mixed stratiform/convective, deep convective and shallow convective. Besides the DSD parameters of gamma distribution, ΔZ_{MP} defined as the difference between a measured radar reflectivity and that from Marshall and Palmer's model was also analyzed. Intraseasonal variation of ΔZ_{MP} was only found at heavy rain. Consistent with the previous study, during the inactive phase, ΔZ_{MP}s were generally positive (broad DSD) and decrease toward negative values (narrow DSD) as the phase of ISV shifts to active ones. We found that a broad DSD and skewed towards higher drop diameters during the inactive ISV phase came mainly from deep convective, while a narrow DSD during the active phase came mainly from shallow convective events. Like surface DSD, mass-weighted mean diameter (D_m) revealed from the EAR measurement was also larger during the inactive phase (deep convective) than that for the active phase (shallow convective). In general, we found that vertical profile of reflectivity gradient (VPRG) from 1.3-GHz wind profiler observations during the inactive phase was larger than for the active phase. This phenomenon may be due to significant coalescence process during the inactive phase.

1. Introduction

One of the most complete descriptions of a rainfall event is given by its drop size distribution (DSD) and its time-space variability (Rosenfeld and Ulbrich, 2003). The DSD reflects the physics of rain. Due to its broad list of applications such as understanding of the microphysical mechanisms responsible for precipitation formation, microwave attenuation by rain, soil erosivity due to rainfall, and retrieval of rainfall properties using radar and other remote sensing techniques, much attention has been focused on observing and modeling DSD.

To study dynamical and electrodynamical coupling process in the equatorial atmosphere over the Indonesian maritime continent, the Coupling Processes in the Equatorial Atmosphere (CPEA) project carried out a first observation campaign (CPEA-I) from April 10 to May 9, 2004 at Kototabang and surrounding area (Fukao, 2006). During the campaign, a clear transition of intraseasonal variation (ISV), in response to Madden–Julian oscillation, hereinafter MJO (Madden and Julian, 1971, 1972), from convectively inactive (April 10–22) to convectively

* Corresponding author. Institute of Broadband Communication, Graz University of Technology, Austria.
E-mail address: marzuki@fmipa.unand.ac.id (Marzuki).

0169-8095/$ – see front matter © 2010 Elsevier B.V. All rights reserved.
doi:10.1016/j.atmosres.2010.03.002

active one (April 23–May 6) was observed (Fukao, 2006; Shibagaki et al., 2006). By using ΔZ_{MP} defined as the difference between a measured radar reflectivity in dB and that from Marshall and Palmer's model ($Z=200R^{1.6}$) as the DSD parameter, Kozu et al. (2005) found that during the inactive phase of ISV, ΔZ_{MP}s were generally positive, indicating that the DSDs were broader than Marshall and Palmer's model (MP model). Recently, Kawashima et al. (2006) found that top-heights of intense echo were suppressed during the active phase compared with that in the inactive phase. Therefore, the results in Kozu et al. (2005) are probably influenced by the dependence of the DSD with the precipitation type (e.g., deep vs. shallow convective) because their analysis was only based on the rainfall intensity.

This paper presents a comprehensive follow-up of Kozu et al. (2005), the characteristics of DSD aloft as well as at the ground level was studied using a 2D-Video Disdrometer (2DVD) and two ground-based atmospheric radars. In addition to ΔZ_{MP} defined by Kozu et al. (2005), a modified gamma distribution was used to parameterize the DSD. By using the 1.3-GHz wind profiler observations, precipitation was partitioned into four categories (i.e., stratifrom, mixed stratiform/convective, deep convective and shallow convective) based on the method in Williams et al. (1995). The DSD parameters within the same rain type during the inactive ISV phase were compared with that during the active one. The possible microphysical processes affecting the DSD during drop fall were deduced from the vertical profile of DSD and radar reflectivity derived from the Equatorial Atmospheric Radar (EAR) and the 1.3-GHz wind profiler observations, respectively.

2. Data description and analysis method

2.1. 2DVD and parameterization of DSD

The DSD observation at the ground was from a 2DVD. The components and measuring principles of this instrument were given by Schönhuber et al. (2008). Drops smaller than 0.2 mm are measured unreliably as found in Tokay et al. (2001) and hence, disregarded in this study. We constructed the DSD for two-minute intervals, adopting a 0.1 mm channel interval from 0.25 mm to 7.45 mm. We disregarded the data in cases of rainfall rates less than 0.1 mm/h.

The raindrop size distribution (DSD) is commonly denoted by $N(D)$ in unit of $1/m^3mm$ where $N(D)dD$ is the number of drops of diameter D to $D+dD$ mm per unit volume (m^3) of air. Here, the DSD was parameterized by a modified gamma distribution as (Kozu and Nakamura, 1991)

$$N(D) = \frac{N_T \Lambda^{\mu+1}}{\Gamma(\mu+1)} D^{\mu} e^{-\Lambda D}, \tag{1}$$

where D (mm), N_T ($1/m^3$), μ, Λ (1/mm) and $\Gamma(y)$ are the drop diameter, the total number of raindrops, shape parameter, slope of the distribution and the complete gamma function, respectively. The DSD parameters of Eq. (1) were estimated by employing the third (M_3), the fourth (M_4), and the sixth (M_6) moment of DSD, as given by

$$\mu = \frac{11\eta - 8 + \sqrt{\eta(\eta+8)}}{2(1-\eta)}, \tag{2}$$

$$\eta = \frac{M_4^3}{M_3^2 M_6}, \tag{3}$$

$$\Lambda = \frac{(\mu+4)M_3}{M_4}, \tag{4}$$

$$N_T = \frac{\Lambda^3 M_3 \Gamma(\mu+1)}{\Gamma(\mu+4)}. \tag{5}$$

The temporal variation of two more parameters, namely σ and D_m were also analyzed. σ is the parameter of lognormal distribution which reflects the standard deviation of the DSD about the geometric mean diameter (Feingold and Levin, 1986). D_m is mass-weighted mean diameter which is defined as the ratio of the fourth and third moment of the DSD ($D_m = \frac{M_4}{M_3}$). It provides information of the skewness (asymmetry) of the DSD.

The rainfall rate (mm/h) is expressed in terms of the DSD as

$$R = 6\pi.10^{-4} \int_0^{\infty} D^3 v(D) N(D) dD, \tag{6}$$

where $v(D)$ is the raindrop fall speed in still air. The fall speed is approximated by the empirical form as (Atlas et al., 1973),

$$v(D) = 9.65 - 10.3e^{(-0.6D)}(\rho/\rho_0)^{0.4}, \tag{7}$$

where ρ_0 and ρ are the air densities at sea level and at altitude (865 m at Kototabang), respectively.

2.2. Radar measurements

Table 1 summarizes system specification of radars used in this study. The characteristics and performance of the wind profiler and EAR observations were described in detail by Gage et al. (1994) and Fukao et al. (2003), respectively. The 1.3-GHz wind profiler used here is located at Global Atmosphere Watch (GAW) observatory of Indonesian Meteorology and Geophysics Agency (BMG), about 300 m away from the EAR site.

The wind profiler echoes were considered as the echoes from precipitation, if rain at the ground surface was detected by the 2DVD. To ensure that both instruments (2DVD and 1.3-GHz wind profiler) are simultaneously observing rain, the observations are screened to require that the profiler has reflectivities greater than 18 dBZ and mean downward Doppler velocities greater than 3 m/s as in Renggono et al. (2001), while the 2DVD is required to have observed at least 0.1 mm/h rainfall rate in the minute sample. To determine the precipitating cloud type, we used 2-min averaged reflectivity,

Table 1
Radar specifications.

Radar parameters	1.3-GHz wind profiler	EAR
Radar system	Pulse Doppler radar	Pulse Doppler radar
Operating frequency	1.3 GHz	47.0 MHz
Transmit power	1.1 kW	100 kW
Antenna	5.9 m^2	110 m in diameter
Beam width	4.1°	3.4°
Range resolution	150 m	150 m

Please cite this article as: Marzuki, et al., Raindrop size distributions of convective rain over equatorial Indonesia during the first CPEA campaign, Atmos. Res. (2010), doi:10.1016/j.atmosres.2010.03.002

Doppler velocity and spectral width derived from the vertical beam with vertical domain extended from 0.75 km to 9.75 km above ground level (AGL). Precipitations were divided into four categories of rainfall (i.e., stratifrom, mixed stratiform/convective, deep convective and shallow convective) based on the algorithm developed by Williams et al. (1995). Tokay and Short (1996) found that all the spectra were found to be convective when rainfall rates were larger than 20 mm/h. Therefore, we included this rainfall rate threshold in our classification algorithm.

Techniques for retrieving the DSD using the VHF Doppler radar have been developed by many investigators over the past decades (e.g., Wakasugi et al., 1986; Sato et al., 1990)). We used a non linear least square fitting based parametric estimation developed by Kozu et al. (1997), to retrieve the DSD from the EAR. Radiosonde data show the 0 °C isotherm level over Kototabang is located approximately at 4 km AGL. Hence, for the purpose of the present work, only the data of vertical beam, starting from 2.04 km and extending upward to 3.24 km AGL were analyzed. We restricted our DSD analysis from the EAR data to a maximum height of 3.24 km (about 1 km below melting layer) to avoid the ice contamination in the DSD spectra.

3. Results

3.1. Daily rainfall and precipitating cloud occurrence during CPEA-I

Fig. 1a shows the surface daily rainfall observed by a Mobile Automatic Weather Station (MAWS) during CPEA-I. On April 21–22, the MAWS data were not available. Dashed line is the time plot of the equivalent black body temperature (TBB) along 0.20°S latitude of radar site with spatial and time resolutions of 1° longitude × 1° latitude and one day, respectively. The TBB data are from GOES-9 satellite observation. Rainfall events were observed almost every day. The largest amount of rainfall (≃43 mm/day) was observed on April 23. Relatively large amount of rainfall (≃30 mm/day) was also observed on May 5. Therefore, it can be concluded that rainfall events at Kototabang are strongly modulated by ISV in which high rainfall totals occurred when super cloud clusters (SCCs) passed over the observation site.

During the campaign (April 10 to May 09), total rainfall measured by the 2DVD were sufficiently accurate and variation of precipitation over the 300 m distance between 2DVD and 1.3-GHz wind profiler (or MAWS) was not significant and can be disregarded. Rainfall totals observed by the MAWS and the 2DVD are 232.72 mm and 223.46 mm, respectively. The difference in the total accumulation of rainfall was mainly due to the technical problem of the 2DVD on April 14, 17 and May 5.

Two minutes averaged data produced a dataset consisting of 1140 simultaneous 2DVD and 1.3-GHz wind profiler observations. Fig. 1b shows the intraseasonal variation of precipitation types during the campaign. Rain duration was very short (less than one hour) during the inactive phase. Consequently, the number of the data during this phase was so small that difficult to observe the variation of precipitation types. However, we found that most of the precipitation type was deep convective. During the active phase, rain duration was very long. Therefore, the variation of precipitation types was more obvious. Stratiform events were dominant during SCC1 and SCC2. Some deep, shallow and mixed stratiform/convective events were also observed during SCC1. During SCC3 (May 5–6), precipitation was dominated by shallow

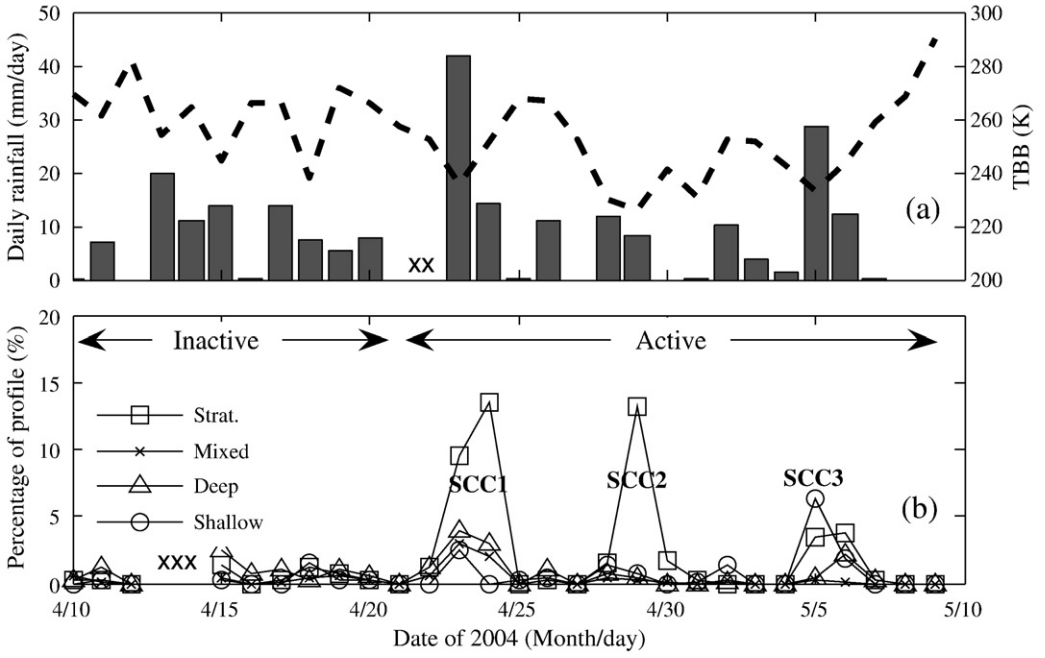

Fig. 1. Surface instrument (MAWS)-based daily rainfall information (a) and the intraseasonal variation of precipitating cloud types during April 10 to May 9, 2004 at Kototabang (b). Dashed line is the time plot of the TBB along 0.20°S latitude of radar site with spatial and time resolutions of 1° longitude × 1° latitude and one day, respectively, and x denotes missing data. The percentage is the ratio of a particular rain type for a particular day to the total observations (1140 profiles).

Please cite this article as: Marzuki, et al., Raindrop size distributions of convective rain over equatorial Indonesia during the first CPEA campaign, Atmos. Res. (2010), doi:10.1016/j.atmosres.2010.03.002

convective events. Some stratiform and deep convective events were also observed in this period. The data number for SCC3 may be reduced by the technical problem of 2DVD on May 5 from 20:00 local time (LT). With the availability of precipitation types during the inactive and active phase, we can then compare the DSD characteristics in each phase.

3.2. Surface DSD

We revisit first the temporal variation of ΔZ_{MP} as reported by Kozu et al. (2005). Considering that the most direct DSD parameter for remote sensing application is the Z–R relation, they defined ΔZ_{MP} as

$$\Delta Z_{MP} = dBZ(measured) - 10log_{10}\left(200R^{1.6}\right), \quad (8)$$

where R is rainfall rate in mm/h. The coefficient and exponent of Z–R relations depend on the precipitation type and geographical locations (Battan, 1973). Therefore, we classified ΔZ_{MP} based on the precipitation type. Each type was then classified into three R categories, i.e., $0.1<R\leq 5$, $5<R\leq 20$ and $R>20$, respectively. Our DSD data are different from that in Kozu et al. (2005) for some points. First, we analyzed the data from simultaneous 2DVD and 1.3-GHzwind profiler observations. Second, we excluded the 2DVD data on April 13 and 14, because there was no BLR observation on these days. Finally, five consecutive DSDs were moving-averaged in Kozu et al. (2005). Because we analyzed the data from simultaneous 2DVD and 1.3-GHz wind profiler observations, moving-average procedure for DSDs was not applied in the present work. Therefore, the data number in the present work is smaller than in Kozu et al. (2005).

Fig. 2 shows the temporal evolution of ΔZ_{MP} for each rain type. There is no stratiform data in Fig. 2c, because $R>20$ in our precipitation classification was categorized as convective, as in Tokay and Short (1996). Although it is not uniform, ΔZ_{MP}s of light rain (Fig. 2a), in general, are positive especially for stratiform rain. This feature did not surprise because MP model was generated from stratiform rain; therefore the Z–R relations from stratiform events were close to this model (e.g., Atlas and Chmela, 1957; Fujiwara, 1965)). Moreover, Tokay and Short (1996) showed higher reflectivities in stratiform rain ($Z=367R^{1.30}$) as compared with that in convective rain ($Z=139R^{1.43}$), for a given rainfall rate. Precipitation from shallow clouds over the tropical

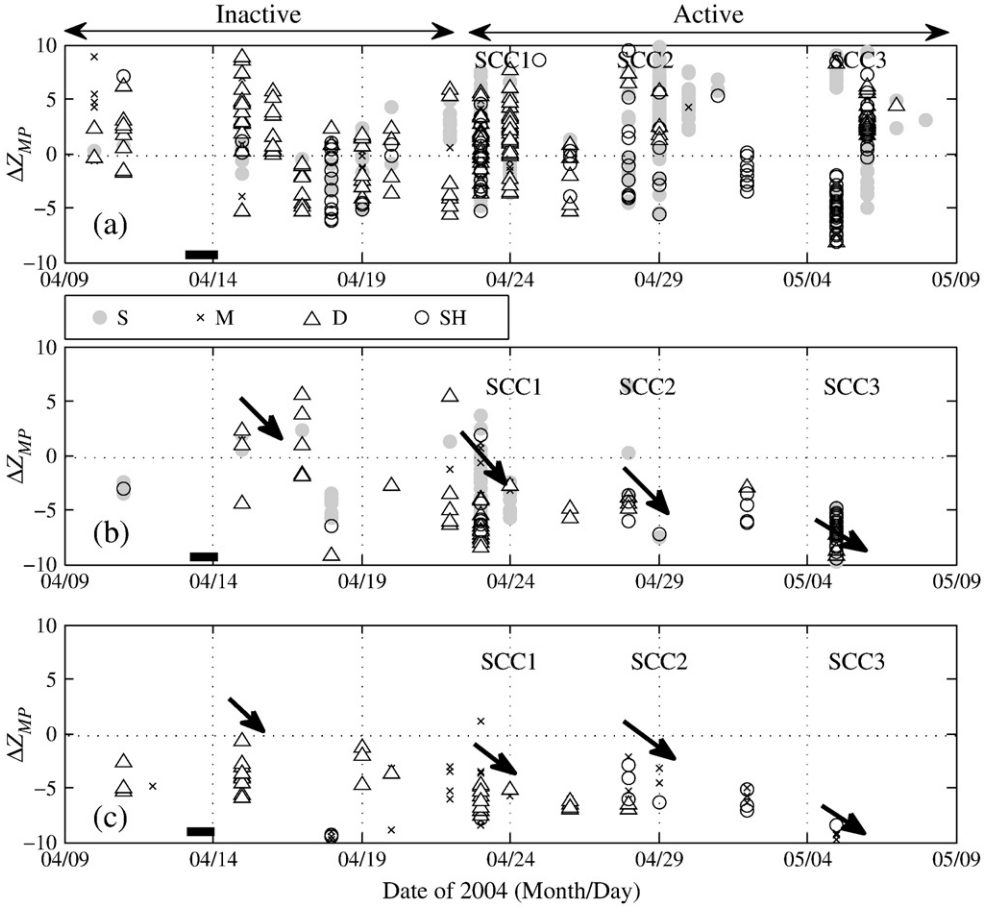

Fig. 2. Temporal evolution of ΔZ_{MP} of each rain type for a particular rainfall rate (R); $0.1<R\leq 5$ (a), $5<R\leq 20$ (b) and $R>20$ (c). Negative (positive) values denote that the DSDs are narrower (broader) than MP model. S, M, D, and SH denote stratiform, mixed stratiform/convective, deep convective and shallow convective rain, respectively. Bold lines at April 13–14 denote missing data.

Please cite this article as: Marzuki, et al., Raindrop size distributions of convective rain over equatorial Indonesia during the first CPEA campaign, Atmos. Res. (2010), doi:10.1016/j.atmosres.2010.03.002

and subtropical oceans generally occurs in the form of light rain/drizzle from stratocumulus/stratus (Austin et al., 1995) and as showers from well-developed trade wind cumuli (Baker, 1993). Thus, a large amount of shallow convective data go to light rain (Fig. 2a). In general, ΔZ_{MP} of heavy rain are negative (Fig. 2b–c), indicating that DSDs are narrower than MP model.

Intraseasonal variation of ΔZ_{MP} for light rain is not obvious (Fig. 2a). Negative and positive values of ΔZ_{MP} for each rain type are observed both in the inactive and the active ISV

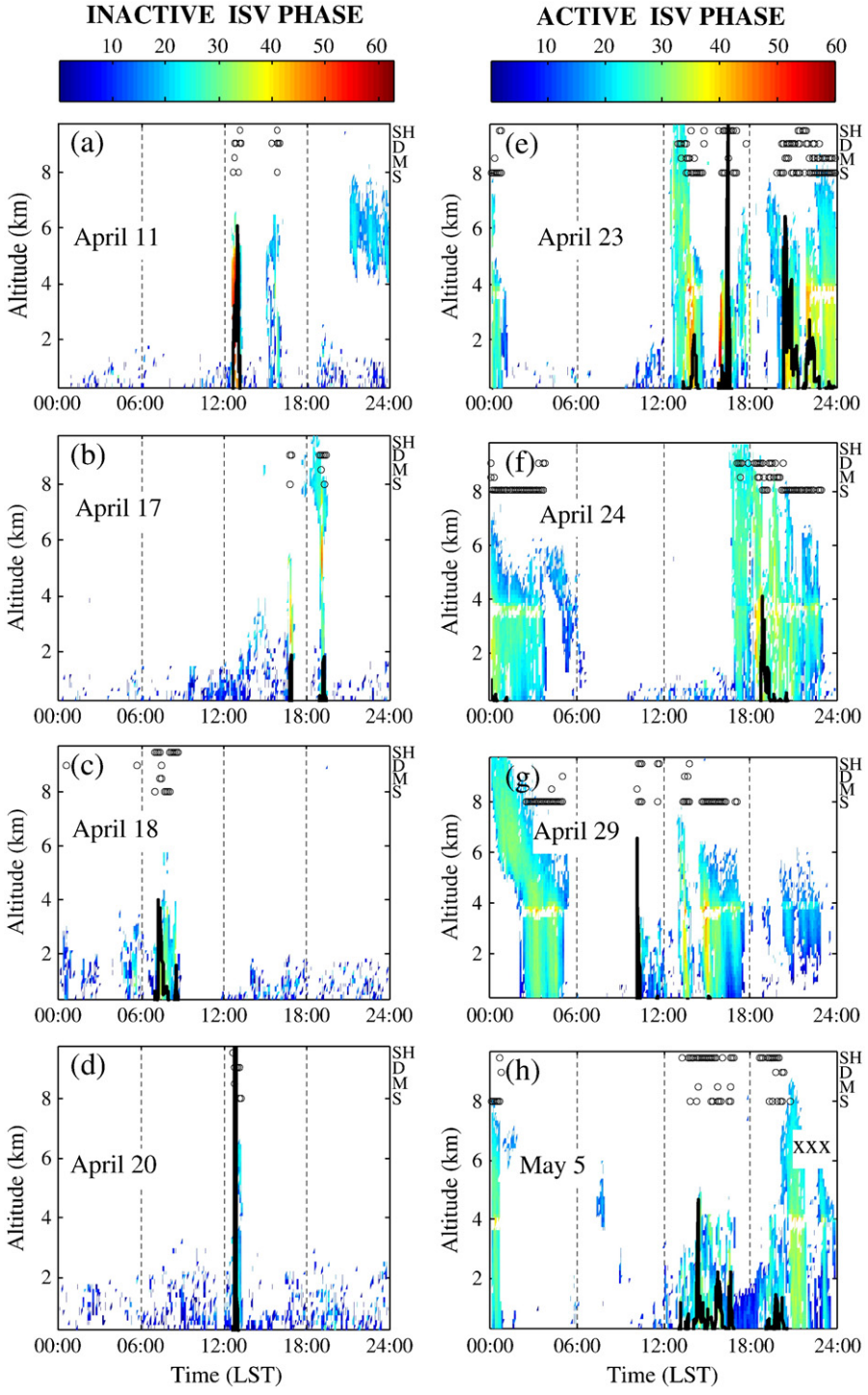

Fig. 3. Time-height cross section of the radar reflectivity (dBZ) from the 1.3-GHz wind profiler observation for several selected days during the inactive and active ISV phase. Black line is surface rainfall rate (R/10 scale, where R is in mm/h). S, M, D and SH denote stratiform, mixed stratiform/convective, deep convective and shallow convective rain, respectively. xxx on May 5 indicates missing data.

Please cite this article as: Marzuki, et al., Raindrop size distributions of convective rain over equatorial Indonesia during the first CPEA campaign, Atmos. Res. (2010), doi:10.1016/j.atmosres.2010.03.002

phase. Light shallow convective has negative ΔZ_{MP} on May 5, but shifts to positive values on May 6. Although ΔZ_{MP} scattered widely as in Kozu et al. (2005), we observed the intraseasonal variation of ΔZ_{MP} at heavy rain (Fig. 2b–c). In the inactive phase, ΔZ_{MP} are generally positive, while they decrease toward negative values as the phase of ISV shifts to active ones. Some ΔZ_{MP} of stratiform events on April 23 are still positive (Fig. 2b), but those of convective events are mostly negative. One of the advantage of this work is we can study the contribution of a particular precipitation type to the ΔZ_{MP} variation described in Kozu et al. (2005). It is observed that relatively positive ΔZ_{MP} in the inactive phase comes from deep convective events. On the other hand, negative ΔZ_{MP} during the active phase mainly comes from shallow convective events especially during SCC2 and SCC3. It should be noted that deep convective events on April 13 and 14 on which many positive values of ΔZ_{MP} in Kozu et al. (2005) was generated, are excluded in the present work.

For closer look at the convective characteristics, the time-height cross section of the precipitation systems for selected days during the inactive and the active ISV phase observed by 1.3-GHz wind profiler along with the precipitation types are shown in Fig. 3. As was also seen in Fig. 3, Kawashima et al. (2006) found that SCC1 was well organized and had stratiform and convective clouds (Fig. 3e–f), as compared to SCC2 (Fig. 3 g) and SCC3 (Fig. 3 h) that had more (less) regions of stratiform (convective) clouds. Alexander et al. (2006) have shown that the most intense diurnal variability in convection occurred during the afternoon, as shown by the larger average of the X-band Doppler Radar reflectivity profiles over the entire CPEA-I campaign. Precipitation echo tops were highest at 17:00 LT, when they reached about

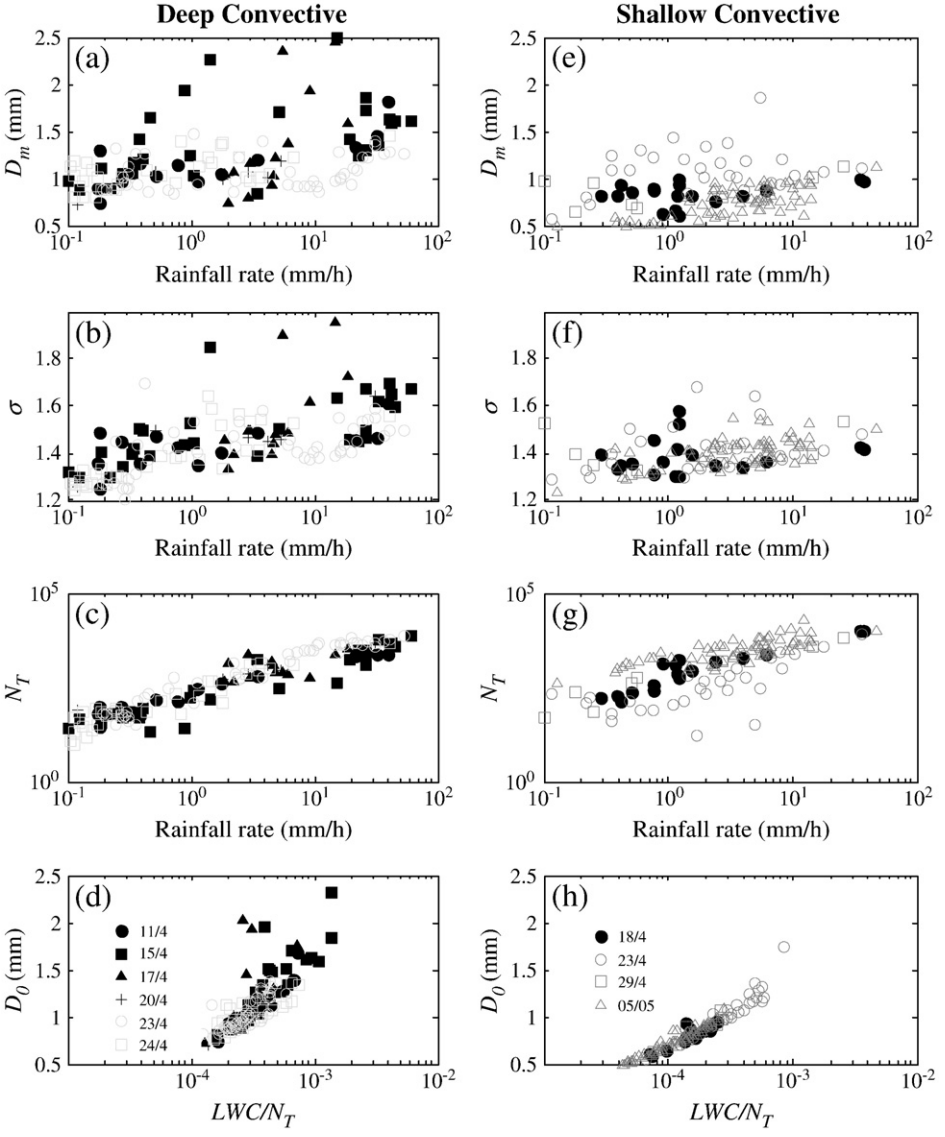

Fig. 4. Scatterplots of parameters of surface DSD for deep and shallow convective rain. Black and gray symbols represent the inactive and the active ISV phases, respectively.

Please cite this article as: Marzuki, et al., Raindrop size distributions of convective rain over equatorial Indonesia during the first CPEA campaign, Atmos. Res. (2010), doi:10.1016/j.atmosres.2010.03.002

15 km. The diurnal variation of precipitation occurrence is also obvious in Fig. 3. Both in the inactive and the active ISV phase, very little convective activity occurred between 08:00 LT and 12:00 LT. In addition, Kozu et al. (2006) and Marzuki et al. (2009) found significant diurnal variation of the DSD at Kototabang. Hence, we investigated the DSD parameters in each ISV phase for four nonoverlapping time intervals of 6 hours each.

Fig. 4a–d show D_m, σ and N_T plotted versus rainfall rate (R), and D_0 vs. liquid water content (LWC) normalized by N_T for deep convective rain. D_0 which is median volume diameter, was calculated by $D_0 = (3.67 + \mu)/\Lambda$. The DSD parameters on April 11, 15, 17 and 20 are plotted as events of the inactive phase, while those on April 23 and 24 are plotted as events of the active ISV phase. Although some differences in the DSD parameters during the active and the inactive phase were observed, we did not find evidence of intraseasonal cycle of the parameters. Fig. 4e–h are the same as in Fig. 4a–d but for shallow convective events. It is again observed that the DSD parameters of shallow convective rain during the inactive phase are not significantly different from that for the active phase. However, if we join Fig. 4a–d (deep convective) and Fig. 4e–h (shallow convective), intraseasonal variation of the DSD parameters can be more obvious (Fig. 5). D_m and σ of deep convective during the inactive phase were larger than those of shallow convective in the active phase. Moreover, N_T of deep convective in the inactive phase is smaller than that in the active phase (shallow convective). When seen in conjunction with the values of N_T, D_m and σ, a broadening of the DSD spectrum during the inactive phase was due to the large population of large-sized drops. This feature is consistent with the characteristics of ΔZ_{MP} discussed above.

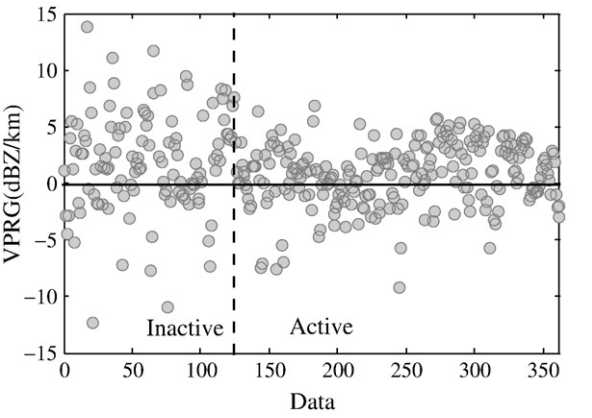

Fig. 6. Temporal evolution of vertical profile of reflectivity gradient (VPRG) for all profiles of convective rain in the range of 1.0–3.0 km AGL (2-min resolution for each data). Negative (positive) values denote downward decreasing (increasing) of radar reflectivity.

3.3. Vertical profile of DSD

Large-sized drops have a disproportionate effect on reflectivity ($Z \simeq D^6$, where D is drop diameter), therefore, their evolution in rain column causes downward increasing or decreasing of radar reflectivity (e.g., (Schumacher et al., 2003; Thurai et al., 2003). Fig. 6 shows the temporal evolution of vertical profile of radar reflectivity gradient (VPRG) for all profiles of convective rain in the range of 1.0–3.0 km AGL. VPRG was calculated by using linear least square fitting of dBZ as function of height. Positive (negative) gradient indicates downward increasing (decreasing) of reflectivity (Hirose and Nakamura, 2002). Although it is not uniform, in general, we

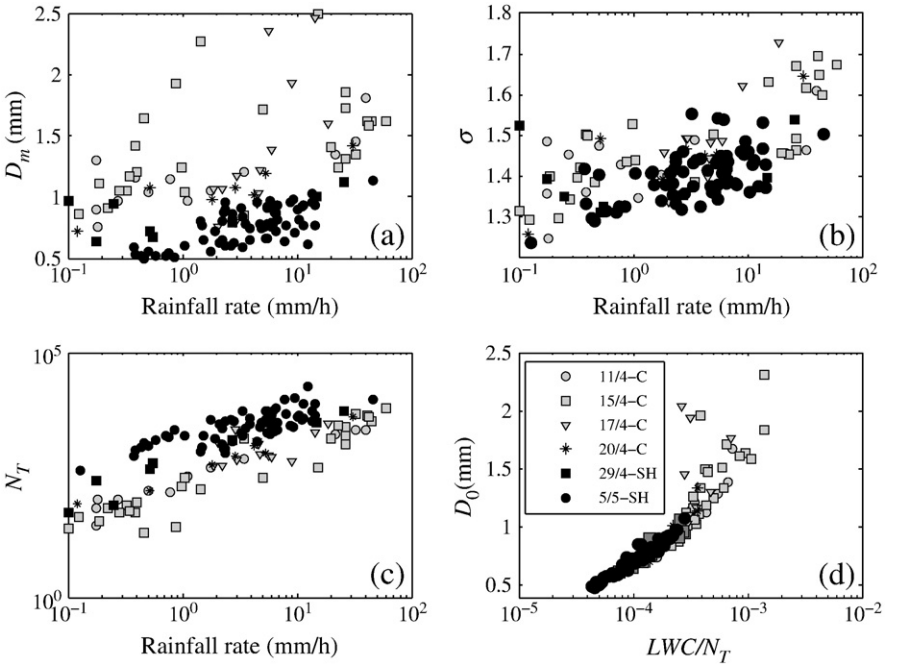

Fig. 5. Same as in Fig. 4 but deep convective events in Fig. 4a–d and shallow convective in Fig. 4e–h are plotted together. Gray and black symbols represent the inactive and the active ISV phases, respectively.

Please cite this article as: Marzuki, et al., Raindrop size distributions of convective rain over equatorial Indonesia during the first CPEA campaign, Atmos. Res. (2010), doi:10.1016/j.atmosres.2010.03.002

found that the VPRG values during the inactive phase (mostly deep convective) are larger than for the active ISV phase (mostly shallow convective). The average (standard deviation) of VPRG during the inactive and the active phase are 1.96 (3.89) and 0.96 (2.78) dBZ/km, respectively.

For closer look at the raindrop evolution, in this section the vertical profile of the DSD from the EAR measurements was discussed. Fig. 7 shows the altitude and time evolution of the DSD of deep convective events on April 11, 17 and 20, respectively. Fig. 8 is the same as in Fig. 7, but for rain events on April 23, 29 and May 5 (shallow convective events). Gagin (1980) argued that the deeper the clouds, the greater the number of graupel particles produced, which consequently increase the number concentration of drops. However, our surface DSD result shows that the number concentration of drops of deep convective (inactive phase) is smaller than that for shallow convective events (active phase). Same characteristics are also observed from the EAR observation (Figs. 7 and 8). During the inactive phase, DSD spectra consist of more large-sized drops and fewer small-sized drops than that for the active one. Another interesting result during the inactive phase is that the DSD is already broad aloft (at 2.79 km). This result may reflect the increased growing process of precipitation particles aloft during the inactive phase as predicted by Kozu et al. (2005). Although it was not uniform, downward increasing of large-sized drops was also observed during the inactive phase. This phenomenon may be due to significant coalescence processes.

Surface DSD also shows relatively larger D_m during the inactive phase (mostly deep convective) than for the active one (shallow convective). Fig. 9 shows the profile of averaged D_m estimated from the EAR for several selected days during the inactive and active ISV phase. The temporal change of DSD in convective rain is very high, therefore, the standard deviations of D_m in Fig. 9b are relatively large. Downward increasing gradients of D_m in Fig. 9a are 0.12 (4/11), 0.16 (4/17), 0.33 (4/20), 0.11 (4/23-1), 0.08 (4/23-2), 0.16 (4/29), 0.15 mm/km (5/5), respectively. Although the difference in gradients of D_m between the inactive and active phase was not significant, we observed that D_m was larger during the inactive phase (deep convective) than for the active phase (shallow convective) as also previously inferred from surface DSD.

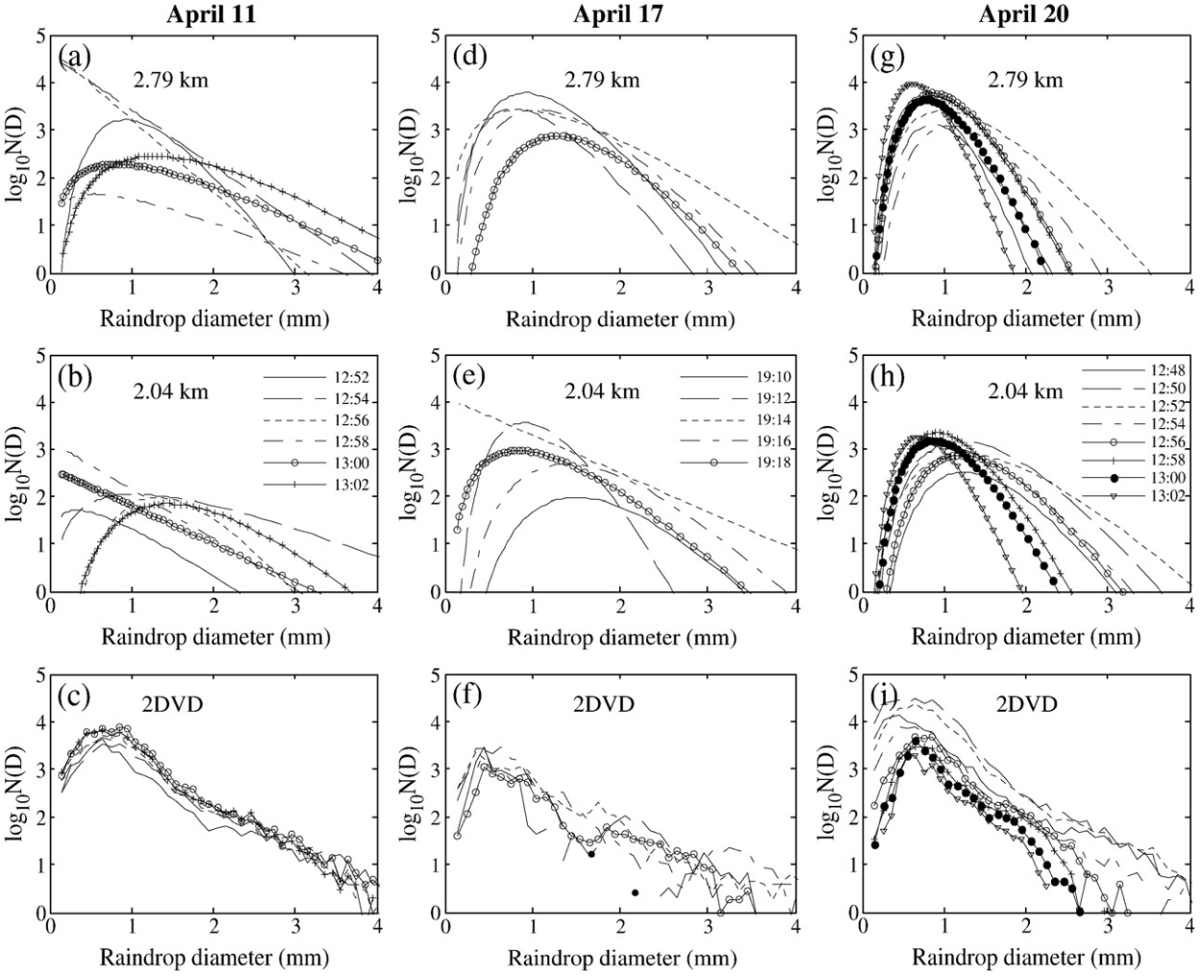

Fig. 7. The altitude and temporal variation of the DSD derived from the EAR measurement for rain events on April 11, 17 and 20. All events are deep convective rain.

Please cite this article as: Marzuki, et al., Raindrop size distributions of convective rain over equatorial Indonesia during the first CPEA campaign, Atmos. Res. (2010), doi:10.1016/j.atmosres.2010.03.002

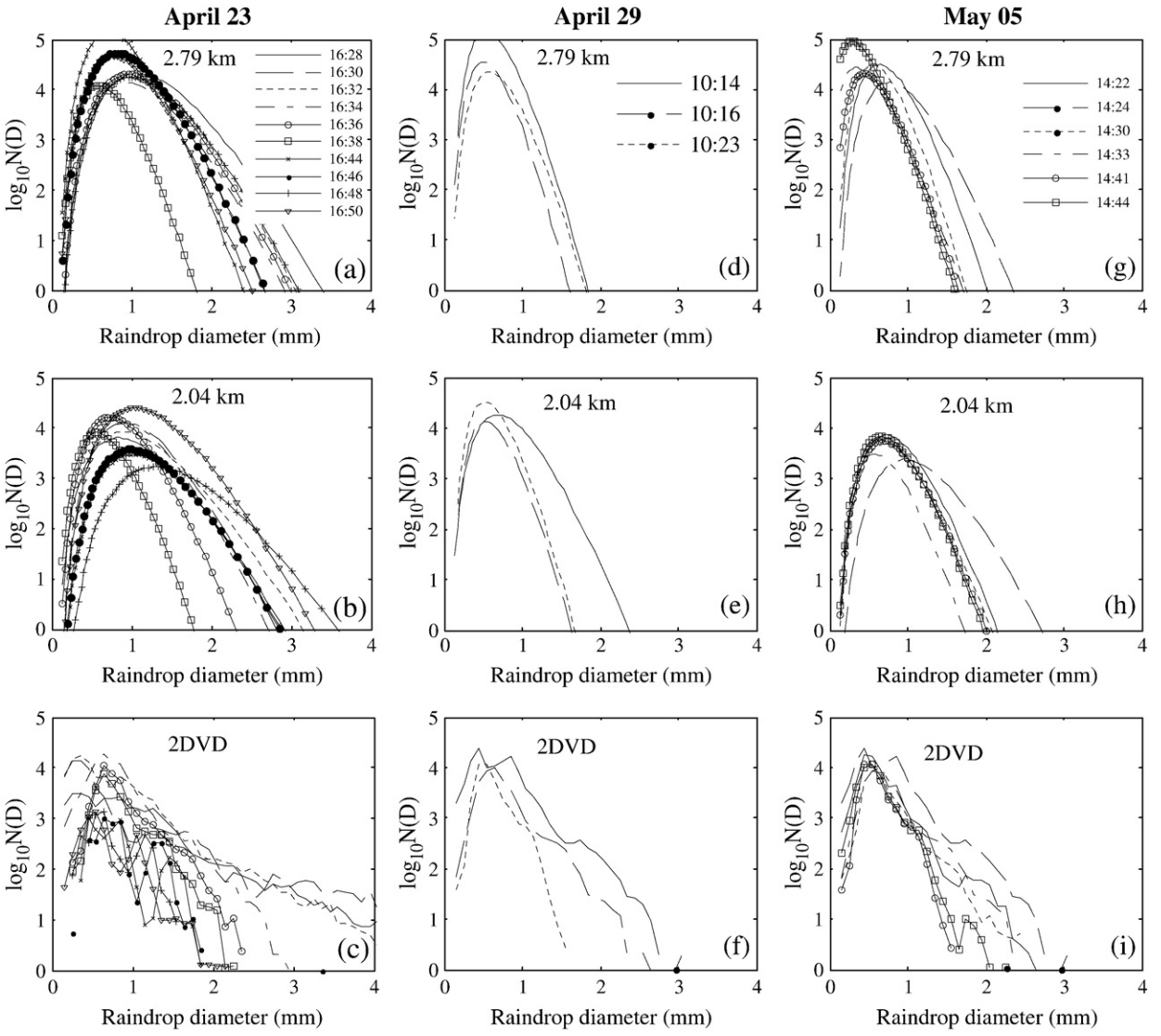

Fig. 8. The altitude and temporal variation of the DSD derived from the EAR measurement for rain events on April 23, 29 and May 05. All events are shallow convective rain.

4. Discussions

The DSD characteristics observed in the inactive and the active phase cannot be totally explained with the available data, and will be the subject for future research work. The increase in solar radiation and ground temperature during the inactive phase, as pointed out by Kozu et al. (2005), may generate more evaporation of small-sized drops. Consequently a deficit of small raindrops in the inactive phase were observed. Large drops in the inactive phase can be developed by the accretion process. However, accretion of cloud droplets by raindrops acts to increase the size of all particles (Rosenfeld and Ulbrich, 2003) and it was not observed in Fig. 7. One alternate mechanism is the large-sized drops increased by coalescence process as mentioned in Section 3.3. High concentration of small-sized drops during the active phase is thought to be due to the breakup process. Drops of 4–5 mm are not disintegrated by spontaneous breakup (Pruppacher and Klett, 1998), therefore, this variation would be due to the collision-induced breakup.

During the active ISV phase especially during the passage of SCC3, strong updrafts were present, indicating the orographic lifting due to the lowest-level westerly wind (Shibagaki et al., 2006). Orographic lifting can supply a large amount of condensates, which create a large number of small-sized drops that fall to the mountain slope (Rosenfeld and Ulbrich, 2003). Moreover, updraft and downdraft can dramatically generate collision. Collision-induced breakup will increase the concentration of small drops. As was discussed above, during the active phase of MJO, increases in the low-level zonal wind (westerly) were observed associated with the passages of SCCs. Westerly wind intensified at the passages of SCC3 and regarded as a westerly wind burst (e.g., (Shibagaki et al., 2006; Kawashima et al., 2006)). Some wind tunnel studies have shown that horizontal wind influenced the DSD and its kinetic

Please cite this article as: Marzuki, et al., Raindrop size distributions of convective rain over equatorial Indonesia during the first CPEA campaign, Atmos. Res. (2010), doi:10.1016/j.atmosres.2010.03.002

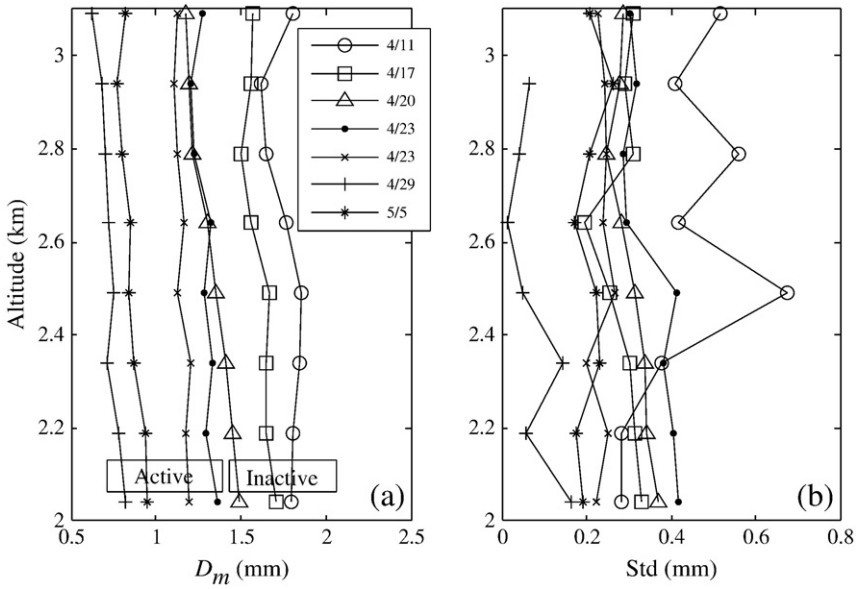

Fig. 9. The vertical profile of averaged D_m (a) and its standard deviation (b) estimated from the EAR for several selected days during the inactive and active phase of ISV. During the inactive phase, all events are deep convective, while during the active ISV phase, all events are shallow convective rains with the exception on April 23 in which lines with × and • denote shallow and deep convective events, respectively.

energy (e.g., Erpul et al., 1998, 2000). (Erpul et al., 1998) obtained a narrower raindrop distribution under wind-driven rain compared to vertical rainfall (without wind). Hence, these two processes may be related to the characteristics of DSD during the active ISV phase at Kototabang.

Vertical profile of DSD was retrieved from a single-frequency profiler at 47 MHz (VHF). Although VHF radars operating at this frequency has an ability to detect simultaneously two separate echoes, one from clear-air turbulence (due to Bragg scattering) and the other from the hydrometeor particles (due to Rayleigh scattering), Rajopadhyaya et al. (1993) showed that the retrieval technique using a VHF radar was unable to resolve small-sized drops accurately. 1.3 GHz wind profiler (UHF radar) may resolve small-sized drops because the radar is very sensitive to Rayleigh scattering from hydrometeor particles. Therefore, in the future, it would be worthwhile to study the DSD characteristics at Kototabang retrieved from dual-frequency profilers at UHF (1.3 GHz wind profiler) and VHF (EAR).

5. Conclusions

This paper is a comprehensive follow-up of the previous study on the intraseasonal variation of DSD at Kototabang. With simultaneous observations of 2DVD and 1.3-GHz wind profiler, we can study not only rainfall rate dependence of the DSD but also the precipitation type dependence. Intraseasonal variation of ΔZ_{MP} was only obvious at heavy rain. Consistent with the prior work, during the inactive phase, ΔZ_{MP}s were generally positive and decrease toward negative values as the phase of ISV shifts to active ones. The interesting result is that we observed the contribution of a particular rain type to this variation. Positive ΔZ_{MP} (broad DSD) during the inactive phase in prior work, comes from deep convective events and negative values (narrow DSD) during the active phase mainly come from shallow convective events. The DSD parameters of gamma distribution provided further evidence. N_T of shallow convective events (in the active phase) was larger than that for deep convective (in the inactive phase). Moreover, D_m in the inactive phase was also larger than that for the active phase and it is consistent with the vertical profile of D_m estimated from the EAR. In general, we found that the VPRG values during the inactive phase (mostly deep convective) are larger than for the active phase (mostly shallow convective) which may be due to significant coalescence process during the inactive ISV phase. In the future, because vertical structure of convective events is complicated, more study is needed to fully understand the microphysical process affecting the formation and evolution of raindrop in term of MJO phases.

Acknowledgements

We are grateful to Dr. Shuichi Mori of IORGC/JAMSTEC who kindly made the MAWS data available. The CPEA project has been supported by Grant-Aid for Scientific Research on Priority Areas funded by the Ministry of Education, Culture, Sports, Science, and Technology (MEXT). The present study was partially supported by Grant for Young Lecturer-2007 of the Indonesian Ministry of Education. This work was also supported in part by the Research Institute for Sustainable Humanosphere (RISH), Kyoto University under Collaborative Research based on Equatorial Atmosphere Radar (EAR) under Grant 2008-E27.

References

Alexander, S., Tsuda, T., Furumoto, J., Shimomai, T., Kozu, T., Kawashima, M., 2006. A statistical overview of convection during the first CPEA campaign. J. Meteor. Soc. Japan 84A, 57–93.

Please cite this article as: Marzuki, et al., Raindrop size distributions of convective rain over equatorial Indonesia during the first CPEA campaign, Atmos. Res. (2010), doi:10.1016/j.atmosres.2010.03.002

Atlas, D., Chmela, A.C., 1957. Physical-synoptic variations of raindrop size parameters. Proc. Sixth Weather Radar Conf. Amer. Meteor. Soc., Cambridge, MA, p. 2130.
Atlas, D., Srivastava, R.C., Sekhon, R.S., 1973. Doppler radar characteristics of precipitation at vertical incidence. Rev. Geophys. Space Phys. 11, 1–35.
Austin, P.M., Wang, Y., Pincus, R., Kujala, V., 1995. Precipitation in stratocumulus clouds: observational and modeling results. J. Atmos. Sci. 52, 2329–2352.
Baker, M., 1993. Trade cumulus observations. The Representation of Cumulus Convection in Numerical Models. : Meteor. Monogr., 46. Amer. Meteor. Soc., pp. 29–37.
Battan, L.J., 1973. Radar Observation of the Atmosphere. University of Chicago Press. 323 pp.
Erpul, G., Gabriels, D., Janssens, D., 1998. Assessing the drop size distribution of simulated rainfall in a wind tunnel. Soil Till. Res. 45, 455–463.
Erpul, G., Gabriels, D., Janssens, D., 2000. Effect of wind on size and energy of small simulated raindrops: a wind tunnel study. Int. Agrophys. 14, 1–7.
Feingold, G., Levin, Z., 1986. The lognormal fit to raindrop spectra from frontal convective clouds in Israel. J. Appl. Meteor. 25, 1346–1363.
Fujiwara, M., 1965. Raindrop-size distribution from individual storms. J. Atmos. Sci. 22, 585–591.
Fukao, S., Hashiguchi, H., Yamamoto, M., Tsuda, T., Nakamura, T., Yamamoto, M.K., Sato, T., Hagio, M., Yabugaki, Y., 2003. Equatorial Atmosphere Radar (EAR): system description and first results. Radio Sci. 38. doi:10.1029/2002RS002767.
Fukao, S., 2006. Coupling Processes in the Equatorial Atmosphere (CPEA): a project overview. J. Meteor. Soc. Japan 84A, 1–18.
Gage, K.S., Williams, C.R., Ecklund, W.L., 1994. UHF wind profilers: a new tool for diagnosing tropical convective cloud system. Bull. Am. Meteorol. Soc. 75, 2289–2294.
Gagin, A., 1980. The relationship between the depth of cumuliform clouds and their raindrop characteristics. J. Rech. Atmos. 14, 409–422.
Hirose, M., Nakamura, K., 2002. Spatial and seasonal variation of rain profiles over asia observed by spaceborne precipitation radar. J. Climate. 15, 3443–3458.
Kawashima, M., Fujiyoshi, Y., Ohi, M., Honda, T., Kozu, T., Shimomai, T., Hashiguchi, H., 2006. Overview of Doppler radar observations of precipitating cloud systems in Sumatera Island during the first CPEA campaign. J. Meteor. Soc. Japan 84A, 33–56.
Kozu, T., Ohno, Y., Reddy, K., 1997. Consideration of raindrop size distribution modeling for wind profiler measurements of precipitation. Proc. the Eight Workshop on Technical and Scientific Aspect of MST radar.
Kozu, T., Nakamura, K., 1991. Rainfall parameter estimation from dual-radar measurements combining reflectivity profile and path-integrated attenuation. J. Atmos. Oceanic Tech. 8, 259–271.
Kozu, T., Shimomai, T., Akramin, Z., Marzuki, Shibagaki, Y., Hashiguchi, H., 2005. Intraseasonal variation of raindrop size distribution at Koto Tabang, West Sumatra, Indonesia. Geophys. Res. Lett. 32, L07803. doi:10.1029/2004GL022340.
Kozu, T., Reddy, K.K., Mori, S., Thurai, M., Ong, J.T., Rao, D.N., Shimomai, T., 2006. Seasonal and diurnal variations of raindrop size distribution in Asian monsoon region. CPEA Special Issue: J. Meteorol. Soc. Japan, 84A, pp. 195–209.
Madden, R.A., Julian, P.R., 1971. Detections of a 40–50 day oscillation in the zonal wind in tropical Pacific. J. Atmos. Sci. 28, 702–708.
Madden, R.A., Julian, P.R., 1972. Description of global scale circulation cells in the tropics with a 40–50 day period. J. Atmos. Sci. 29, 1109–1123.
Marzuki, Kozu, T., Shimomai, T., Randeu, W.L., Hashiguchi, H., Shibagaki, Y., 2009. Diurnal variation of rain attenuation obtained from measurement of raindrop size distributino in equatorial Indonesia. IEEE Trans. Ant. Propag. 57 (4), 1191–1196 Pt.II.
Pruppacher, H.R., Klett, J.D., 1998. Microphysics of Cloud and Precipitation. Kluwer. 954 pp.
Rajopadhyaya, D.K., May, P.T., Vincent, R.A., 1993. A general approach to the retrieval of rain dropsize distributions from wind profiler Doppler spectra: modeling results. J. Atmos. Oceanic Technol. 10, 710–717.
Renggono, F., Hashiguchi, H., Fukao, S., Yamanaka, M.D., Ogino, S.Y., Okamoto, N., Murata, F., Sitorus, B.P., Kudsy, M., Kartasasmita, M., Ibrahim, G., 2001. Precipitating clouds observed by 1.3-GHz boundary layer radars in equatorial Indonesia. Ann. Geophys. 19, 889–897.
Rosenfeld, D., Ulbrich, C.W., 2003. Cloud microphysical properties, processes, and rainfall estimation opportunities. Radar and Atmospheric Science: a collection of essays in honor of David Atlas, Meteor. Monogr. Amer. Meteor. Soc. 52, 237–258.
Sato, T., Doji, H., Iwai, H., Kimura, I., 1990. Computer processing for deriving drop-size distributions and vertical air velocities from VHF Doppler radar spectra. Radio Sci. 25, 961–973.
Shibagaki, Y., Kozu, T., Shimomai, T., Mori, S., Murata, F., Fujiyoshi, Y., Hashiguchi, H., Fukao, S., 2006. Evolution of a super cloud cluster and the associated wind fields observed over the Indonesian Maritime Continent during the first CPEA campaign. J. Meteor. Soc. Japan 84A, 19–31.
Schönhuber, M., Lammer, G., Randeu, W.L., Schönhuber, M., Lammer, G., Randeu, W.L., 2008. The 2-D-video-distrometer, chapter 1 in: precipitation: advances in measurement, estimation and prediction. In: Michaelides, S. (Ed.), Springer. ISBN: 978-3-540-77654-3.
Schumacher, Courtney, Jr, Houze, Robert, A., 2003. Stratiform rain in the tropics as seen by the TRMM precipitation radar. J. Climate. 16, 1739–1756.
Thurai, M., Iguchi, T., Kozu, T., Eastment, J.D., Wilson, C.L., Ong, J.T., 2003. Radar observation in Singapore and their implications for the TRMM precipitation radar retrievel algorithms. Radio Sci. 38. doi:10.1029/2002RS002855.
Tokay, A., Short, D.A., 1996. Evidence from tropical raindrop spectra of the origin of rain from stratiform versus convective clouds. J. Appl. Meteor. 35, 355–371.
Tokay, A., Kruger, A., Krajewski, W.F., 2001. Comparison of drop size distribution measurements by impact and optical disdrometer. J. Appl. Meteor. 40, 2083–2097.
Wakasugi, K., Mizutani, A., Matsuo, M., Fukao, F., Kato, S., 1986. A direct method for deriving drop-size distribution and vertical air velocities from VHF Doppler radar spectra. J. Atmos. Oceanic Technol. 3, 623–629.
Williams, C.R., Ecklund, W.L., Gage, K.S., 1995. Classification of precipitating clouds in the tropics using 915-MHz wind profilers. J. Atmos. Oceanic Technol. 12, 996–1011.

Please cite this article as: Marzuki, et al., Raindrop size distributions of convective rain over equatorial Indonesia during the first CPEA campaign, Atmos. Res. (2010), doi:10.1016/j.atmosres.2010.03.002